J Musculoskelet Neuronal Interact 2018; 18(2):165-175

Journal of Musculoskeletal and Neuronal Interactions JMNI

Original Article

Zoledronic acid prevents disuse osteopenia and augments gene expression of osteoclastic differentiation markers in mice

Jens Bay Vegger, Annemarie Brüel*, Jesper Skovhus Thomsen*

Department of Biomedicine, Aarhus University, Denmark
* Joint senior author

Abstract

Objectives: Disuse is characterized by a rapid and profound bone resorption. Zoledronic acid (Zol) inhibits osteoclastic bone resorption. The aim of the study was to prevent disuse osteopenia with Zol and investigate gene expression markers of osteoclastic differentiation. **Methods:** Disuse osteopenia was induced by injecting botulinum toxin (BTX) into the right hind limb of 16-week-old C57BL/6J female mice. Zol (100 µg/kg) was injected s.c. once at study start. The immobilized bones were investigated with DEXA, microCT, mechanical testing, dynamic bone histomorphometry, and RT-qPCR. **Results:** The BTX-injections resulted in a loss of cortical and trabecular bone as well as mechanical strength compared to intact baseline and control mice. Treatment with Zol prevented the loss of bone and mechanical strength. Interestingly, treatment with Zol resulted in a higher expression of *Nfatc1* and *Dcstamp*, which are markers osteoclastic differentiation. **Conclusions:** Zol effectively prevented BTX-induced disuse osteopenia. Furthermore, gene expression markers of osteoclastic differentiation were increased in Zol treated immobilized mice, indicating that Zol only affect mature bone resorbing osteoclasts *in vivo*. However, the current findings are preliminary and calls for further studies.

Keywords: Immobilization, Zoledronate, microCT, Mechanical Testing, RT-qPCR

Introduction

In mice, many different approaches have been used to study disuse osteopenia, e.g. plaster casting[1], tail suspension[2], and sciatic neurectomy[3]. The present study uses the botulinum toxin (BTX) model, where injection of BTX into the hind limb musculature inhibits release of acetylcholine containing vesicles from the neuromuscular endplate and thereby effectively paralyzes the limb[4-6]. Our lab, as well as others, have extensively investigated the BTX model, and consistently found that the loss of both cortical and trabecular bone reaches a maximum as early as three weeks after the injection of BTX[4,7-10]. Consequently, initiation of bone resorption is rapid and markers of osteoclastic activity are increased already after a week of disuse[10-12].

Antiresorptive drugs are the mainstay for treating osteoporotic patients and the most frequently used are nitrogen-containing bisphosphonates (BPs)[13]. When internalized in the body, BPs accumulate in the skeleton due to their high affinity for hydroxyapatite, and are rapidly cleared systemically by renal filtration. During bone resorption, osteoclasts take up BPs by endocytosis and accumulate them intracellularly[14]. As the intracellular concentration of BPs rises, the enzyme farnesyl pyrophosphate synthase (FPPS) is inhibited. FPPS produces farnesyl pyrophosphate, which is important for prenylation, i.e. protein lipid modification, of lipid-anchored, membrane-attached signaling molecules. Ultimately, loss of prenylation causes disruption of the ruffled border, the cytoskeleton, and intracellular signals leading to inhibition and apoptosis of the bone-resorbing osteoclasts[14].

The newest BP, zoledronic acid (Zol), is a high affinity BP that is administered intravenously. In osteoporotic patients, Zol has to be injected only once yearly compared to prior formulations such as e.g. alendronate, which is administered orally on a weekly basis[13]. We hypothesize that a single injection of Zol prevents BTX-induced disuse osteopenia by inhibiting the associated osteoclastic bone resorption.

It has been speculated that BPs not only affect mature bone resorbing osteoclasts, but also directly influence

The authors have no conflict of interest.

Corresponding author: Jens Bay Vegger, Department of Biomedicine, Aarhus University, Wilhelm Meyers Allé 3, DK-8000 Aarhus C, Denmark
E-mail: jbve@biomed.au.dk

Edited by: P. Makras
Accepted 12 December 2017

osteoclastogenesis[15-17]. The speculations are based on *in vitro* studies, in which BPs are added to cell cultures. However, this approach does not resemble the *in vivo* environment, where BPs binds hydroxyapatite with high affinity and is rapidly cleared systemically by renal filtration. In order to investigate whether the differentiation of osteoclasts is affected by BPs *in vivo*, we hypothesize that gene expression of markers of osteoclastic differentiation are augmented when disuse-induced bone resorption is disrupted by Zol. Higher expression of markers of osteoclastic differentiation during disuse would suggest that mechanosensation of the osteocytic network, production of pro-osteoclastic factors, such as RANKL, and differentiation of osteoclasts are not inhibited by Zol. Accordingly, the aim of the study was to prevent disuse-induced osteopenia with Zol and investigate markers of osteoclastic differentiation in 16-week-old female C57BL/6J mice. The methods used were DEXA, µCT, mechanical testing, dynamic bone histomorphometry, and RT-qPCR.

Materials and methods

Animals

Forty-eight C57BL/6J female mice (Taconic) with a mean body weight of 22.5±1.1 g were housed at 20°C with a 12/12 h light/dark cycle. The animals had free access to tap water and standard mice chow (1324, Altromin).

One week prior to study start, the animals were randomized according to their bodyweight (BW) into four groups (n=12): Base, Ctrl, BTX, and BTX+Zol. At the age of 16 weeks, the mice in the BTX and BTX+Zol groups were injected i.m. with 20 IU BTX (Botox, Allergan) per kg BW, distributed equally into the quadriceps muscle and calf muscles of the right hind limb. The Ctrl group was injected i.m. with saline using the same regimen as the BTX injections. Furthermore, the BTX+Zol group had a one-time s.c. injection with 100 µg Zol (Zoledronic Acid, Actavis) per kg BW. The dosage used is comparable to that used when treating osteoporosis, which corresponds to 71.4 µg Zol per kg BW in a "standard" human with a BW of 70 kg. The Ctrl, BTX, and BTX+Zol groups were injected i.p. with 20 mg alizarin, 20 mg calcein, and 20 mg tetracycline per kg BW 12, 8, and 4 days before euthanasia, respectively. The Base group was euthanized at study start to serve as baseline.

The treatment lasted for three weeks after which the mice were euthanized by anesthesia with 4% isoflurane (IsoFlo Vet, Orion Pharma Animal Health) and removal of the heart. No mice died or were euthanized prematurely.

Immediately after euthanasia, the distal part of the right tibia was isolated, carefully cleaned from soft tissue, snap-frozen in liquid nitrogen and stored at -80°C. The right rectus femoris muscle was isolated and the wet weight determined using an electronic scale. The right femur was isolated, carefully cleaned from soft tissue, and stored in Ringer's solution at -20°C. The experiment complied with the EU Directive 2010/63/EU for animal experiment, and all procedures were approved by the Danish Animal Experiments Inspectorate.

Figure 1. Depicting the analyzed volumes of interest (VOI) from the µCT scans. The green area represents the VOI analyzed at the femoral mid-diaphysis, the blue area represents the VOI analyzed at the distal femoral metaphysis, and the red area represents the VOI analyzed at the distal femoral epiphysis.

Dual Energy X-Ray Absorptiometry (DEXA)

The length of the femur was measured with a digital sliding caliper, and thereafter placed in a DEXA scanner (Sabre XL, Norland Stratec) and scanned with a pixel size of 0.1 mm. The analysis included: Bone mineral content (BMC) and areal bone mineral density (aBMD) for the whole femur. Quality assurance was performed by scans of the two solid-state phantoms provided with the scanner.

Micro Computed Tomography (µCT)

The mid-diaphysis and distal part of the femur was scanned in a desktop µCT scanner (Scanco µCT 35, Scanco Medical AG). The mid-diaphysis was scanned with an isotropic voxel size of 7 µm, X-ray voltage of 55 kV and current of 145 µA, and an integration time of 300 ms, while the distal part of the femur was scanned with an isotropic voxel size of 3.5 µm, X-ray voltage of 55 kV and current of 145 µA, and an integration time of 800 ms.

The femoral mid-diaphysis was analyzed by semi automatically drawing an 819-µm-high volume of interest (VOI), including cortical bone only, with the software provided with µCT scanner (version 6.5, Scanco Medical AG) (Figure 1). The data sets were segmented with a fixed threshold filter (556 mg HA/cm^3). The analysis included: cortical area (Ct.Ar), tissue area (Tt.Ar), cortical area

fraction (Ct.Ar/Tt.Ar), cortical thickness (Ct.Th), marrow area (Ma.Ar), polar moment of inertia (*J*), and tissue mineral density (TMD).

The distal femoral metaphysis was analyzed by semi automatically drawing a 1-mm-high VOI including trabecular bone, but excluding cortical bone, placed 0.2 mm proximal to the growth plate (Figure 1). The data sets were low-pass filtered using a Gaussian filter (σ=1, support=2) and segmented with a fixed threshold filter (454 mg HA/cm^3). The distal femoral epiphysis was analyzed by semi automatically drawing a VOI placed distal to the growth plate and including all trabecular bone until the intercondylar fossa (Figure 1). The 3D data sets were low-pass filtered using a Gaussian filter (σ=1, support= 2) and segmented with a fixed threshold filter (546 mg HA/cm^3). The minimum point between the marrow and the bone peak in the attenuation histograms were automatically determined for the VOIs using IPL (version 5.11, Scanco Medical AG) and the median of these thresholds was used as threshold for the respective VOI. The analysis included: trabecular bone volume fraction (BV/TV), trabecular thickness (Tb.Th), trabecular number (Tb.N), trabecular separation (Tb.Sp), connectivity density (Conn.D), structure model index (SMI), and tissue mineral density (TMD).

The analyzes followed the current guidelines[18]. Quality assurance was performed by weekly (density) and monthly (geometry) scans of the solid-state calibration phantom provided with the scanner.

Mechanical testing

The femur was placed on a custom-made testing jig, supporting the proximal and distal part of the shaft. The distance between the two supporting rods was 7.1 mm. Load was applied with a third rod in an anterior-posterior direction at the midpoint of the femur at a constant deflection rate of 2 mm/min until fracture using a materials testing machine (5566, Instron). Subsequently, the proximal part of the femur was placed in another custom-made fixation jig supporting the shaft under the neck. Load was applied to the top of the femoral head with a constant deflection rate of 2 mm/min until fracture of the femoral neck[19]. The analysis included: Fracture strength and maximum stiffness.

Dynamic bone histomorphometry

After mechanical testing, the distal part of the femur were immersion-fixed in 0.1 M sodium phosphate buffered formaldehyde (4% formaldehyde, pH 7.0) for 48 h, dehydrated in ethanol, embedded undecalcified in methylmetacrylate, and 7-µm-thick sections were cut using a hard tissue microtome (RM 2065, Leica). Sections were mounted unstained on microscope slides and placed in a microscope (Eclipse 80i, Nikon) equipped for fluorescence microscopy. The newCAST stereology system (Version 6.4.1.2240, Visiopharm) was used to count intersections with fluorochrome labels. Briefly, a region of interest (ROI), excluding cortical bone, was placed at the distal femoral epiphysis. Furthermore, a 1000-µm-high ROI, excluding cortical bone and primary spongiosa, was placed 200 µm proximal to growth plate covering the distal femoral metaphysis. At a final magnification of ×580, a line grid was superimposed onto fields of view that covered 100% of the ROI. The line grid was used to count intersections and distances between the fluorochrome labels. The analysis included: Mineralizing surfaces (MS/BS), mineral apposition rate (MAR), and bone formation rate (BFR/BS).

Reverse transcription real-time quantitative polymerase chain reaction (RT-qPCR)

Six tibiae from each group were used for RT-qPCR. The distal half part of the tibia including bone marrow was ground in a 1.5 ml microcentrifuge tube with a micropestle (VWR) at -80°C. Lysis buffer from a PureLink RNA Mini kit (Ambion) was added, and the pulverized bone was homogenized with a rotor/stator homogenizer (VDI 12, VWR). RNA was isolated and purified with the PureLink RNA Mini kit. RNA quality was checked by running 1 µg of total RNA on an agarose gel. 1 µg of total RNA was transcribed into cDNA using qScript cDNA SuperMix (Quanta Biosciences). cDNA was diluted 1:5 with DEPC-treated water and 2 µl diluted cDNA was used in each reaction. PerfeCTa qPCR FastMix II (Quanta Biosciences) and TaqMan Gene Expression Assays (LifeTechnologies) were used with the following amplification protocol; hot start 95°C for 30 s followed by 40 cycles of amplification and quantification at 95°C for 3 s and 60°C for 30 s on a LightCycler 480 (Version 1.5, Roche). The studied genes were *Bglap* (osteocalcin) (Mm03413826_mH), *Ctsk* (cathepsin K) (Mm00484039_m1), *Opg* (Osteoprotegerin) (Mm01205928_m1), *Rankl* (Receptor activator of nuclear factor κ-β ligand) (Mm00441906_m1), *Nfatc1* (Nuclear factor of activated T-cells, cytoplasmic 1) (Mm00479445_m1), and *Dcstamp* (Dendrocyte expressed seven transmembrane protein) (Mm04209236_m1). Each sample was run in triplicates, and normalized to the reference genes *B2m* (beta-2 microglobulin) (Mm00437762_m1) and *Gapdh* (glyceraldehyde-3-phosphate dehydrogenase) (Mm99999915_g1). Data is presented as $-\Delta Ct$ ($-(Ct_{target} - Ct_{reference})$).

Statistics

Data are given as mean ± SD. Differences between the groups were analyzed by a parametric one-way ANOVA, whenever normal distribution requirements were met or otherwise by a non-parametric Kruskal-Wallis test. When significant variance was found, multiple comparisons between the groups were performed with the Student-Newman-Keuls test. Results were defined as statistically significant, if the two-tailed $p<0.05$. The statistical analyzes and graph drawing was performed using SigmaPlot (Version 13.0, Systat Software).

Table 1. Bodyweight (BW) at study start and euthanasia, rectus femoris muscle mass, and length of the femur.

	BW at study start (g)	BW at euthanasia (g)	Change in BW from study start to euthanasia (%)	Rectus femoris muscle mass (mg)	Femur length (mm)
Base	–	22.7 ± 1.2	–	65.5 ± 8.6	15.41 ± 0.25
Ctrl	22.2 ± 1.0	22.2 ± 1.4	0.1 ± 3.4	66.5 ± 8.3	15.56 ± 0.24
BTX	22.2 ± 0.9	20.5 ± 0.7 [a,b]	–7.5 ± 2.6 [b]	34.8 ± 3.8 [a,b]	15.44 ± 0.26
BTX+Zol	22.9 ± 1.4	21.2 ± 1.2 [a,b,c]	–7.1 ± 4.4 [b]	33.8 ± 4.1 [a,b]	15.51 ± 0.32

16-week-old C57BL/6J female mice immobilized with botulinum toxin (BTX) and treated with zoledronic acid (Zol) compared with baseline (Base) and control (Ctrl) mice. [a] denotes a significant difference (p<0.05) from Base, [b] denotes a significant difference (p<0.05) from Ctrl, and [c] denotes a significant difference (p<0.05) from BTX. Mean ± SD.

Table 2. Dual Energy X-ray Absorptiometry (DEXA) of the entire femur.

	BMC (mg)	aBMD (mg/cm² of HA)
Base	15.3 ± 1.1	48.7 ± 2.1
Ctrl	16.5 ± 1.2 [a]	50.2 ± 2.3
BTX	11.2 ± 0.5 [a,b]	39.4 ± 1.0 [a,b]
BTX+Zol	16.0 ± 1.1 [c]	49.5 ± 1.8 [c]

16-week-old C57BL/6J female mice immobilized with botulinum toxin (BTX) and treated with zoledronic acid (Zol) compared with baseline (Base) and control (Ctrl) mice. Bone mineral content (BMC), areal bone mineral density (aBMD), and hydroxyapatite (HA). [a] denotes a significant difference (p<0.05) from Base, [b] denotes a significant difference (p<0.05) from Ctrl, and [c] denotes a significant difference (p<0.05) from BTX. Mean ± SD.

Results

Animals

The BTX-injected mice lost BW from study start to euthanasia (Table 1). Injection of BTX had a profound atrophic effect on the rectus femoris muscle compared to the Base and Ctrl groups (Table 1). Neither BTX nor Zol treatment affected the length of the femur (Table 1).

Dual Energy X-Ray Absorptiometry (DEXA)

The BTX-injections caused a lower BMC and aBMD of the entire femur compared to the Base and Ctrl groups, however, this bone loss was prevented by treatment with Zol (Table 2).

Micro Computed Tomography (μCT)

At the femoral mid-diaphysis, BTX resulted in a smaller Ct.Ar, Ct.Ar/Tt.Ar, and Ct.Th caused by endosteal bone resorption, as the Ma.Ar of the immobilized femora was larger than that of the Base and Ctrl groups (Table 3). Consequently, the BTX-induced loss of cortical bone led to a lower *J* compared to the Base and Ctrl groups (Table 3). Treatment with Zol was able to counteract the deteriorating effects of BTX on cortical bone at the femoral mid-diaphysis (Table 3).

At both the distal femoral metaphysis and epiphysis, injection of BTX caused a lower BV/TV, Tb.Th, Tb.N, and TMD and a higher Tb.Sp compared to the Base and Ctrl groups (Figures 2, 3, and Table 4). Furthermore, at the distal femoral epiphysis, BTX reshaped the trabecular network into a more rod-like structure as indicated by the higher SMI compared to the Base and Ctrl groups (Table 4). In general, treatment with Zol prevented the BTX-induced loss of trabecular bone and microstructure.

Mechanical testing

At both the femoral mid-diaphysis and neck, BTX-injections resulted in substantial lower facture strength and maximum stiffness than the Base and/or Ctrl group (Figure 4). Zol completely prevented the mechanical deterioration inflicted by BTX (Figure 4).

Table 3. Micro Computed Tomography (μCT) of the femoral mid-diaphysis.

	Ct.Ar (mm²)	Tt.Ar (mm²)	Ct.Ar/Tt.Ar (%)	Ct.Th (μm)	Ma.Ar (mm²)	J (mm4)	TMD (mg/cm³ of HA)
Base	0.73 ± 0.03	1.71 ± 0.08	43.0 ± 2.0	160 ± 6	0.97 ± 0.07	0.33 ± 0.03	1145 ± 10
Ctrl	0.77 ± 0.04	1.72 ± 0.07	44.6 ± 1.8	171 ± 8 [a]	0.95 ± 0.05	0.35 ± 0.03	1163 ± 11 [a]
BTX	0.65 ± 0.03 [a,b]	1.68 ± 0.07	38.9 ± 1.3 [a,b]	146 ± 5 [a,b]	1.03 ± 0.05 [a,b]	0.30 ± 0.03 [a,b]	1156 ± 7 [a]
BTX+Zol	0.75 ± 0.03 [c]	1.69 ± 0.06	44.5 ± 1.3 [c]	169 ± 5 [a,c]	0.94 ± 0.04 [c]	0.33 ± 0.03 c	1165 ± 11 [a]

16-week-old C57BL/6J female mice immobilized with botulinum toxin (BTX) and treated with zoledronic acid (Zol) compared with baseline (Base) and control (Ctrl) mice. Cortical area (Ct.Ar), tissue area (Tt.At), cortical area fraction (Ct.Ar/Tt.Ar), cortical thickness (Ct.Th), marrow area (Ma.Ar), polar moment of inertia (J), tissue mineral density (TMD), and hydroxyapatite (HA). [a] denotes a significant difference (p<0.05) from Base, [b] denotes a significant difference (p<0.05) from Ctrl, and [c] denotes a significant difference (p<0.05) from BTX. Mean ± SD.

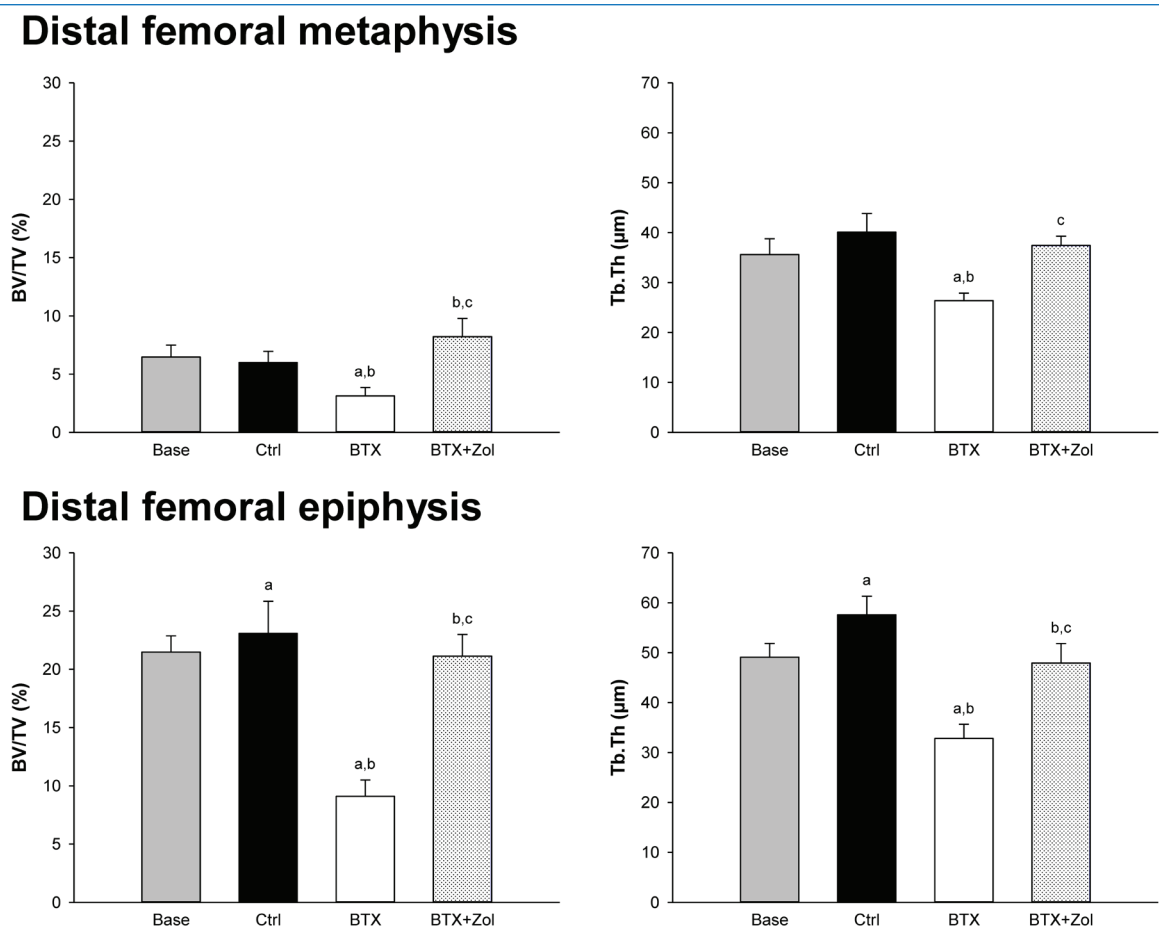

Figure 2. 16-week-old C57BL/6J female mice immobilized with botulinum toxin (BTX) and treated with zoledronic acid (Zol) compared with baseline (Base) and control (Ctrl) mice. Trabecular bone volume fraction (BV/TV) and trabecular thickness (Tb.Th) obtained by µCT at the distal femoral metaphysis and epiphysis. [a] denotes a significant difference (p<0.05) from Base, [b] denotes a significant difference (p<0.05) from Ctrl, and [c] denotes a significant difference (p<0.05) from BTX. Mean ± SD.

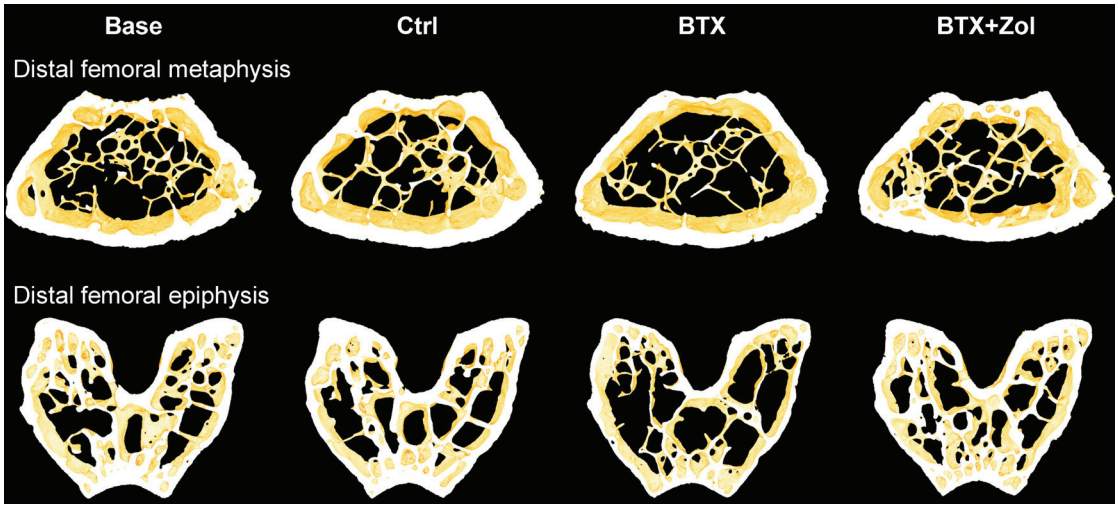

Figure 3. 16-week-old C57BL/6J female mice immobilized with botulinum toxin (BTX) and treated with zoledronic acid (Zol) compared with baseline (Base) and control (Ctrl) mice. 3D images of the distal femoral metaphysis and epiphysis. Samples were chosen based upon the mean values of the groups. The distal femoral metaphysis and epiphysis are not scaled relatively to each other.

Table 4. Micro Computed tomography (μCT) of the distal femoral metaphysis and epiphysis.

	Tb.N (1/mm)	Tb.Sp (μm)	Conn.D (1/mm³)	SMI (–)	TMD (mg/cm³ of HA)
Distal femoral metaphysis					
Base	3.56 ± 0.19	281 ± 15	187 ± 39	2.12 ± 0.18	874 ± 13
Ctrl	3.30 ± 0.25 [a]	304 ± 23 [a]	135 ± 30 [a]	2.26 ± 0.24	891 ± 10 [a]
BTX	3.00 ± 0.25 [a,b]	331 ± 27 [a,b]	112 ± 35 [a]	2.34 ± 0.16 [a]	844 ± 10 [a,b]
BTX+Zol	3.49 ± 0.26 [c]	287 ± 20 [c]	153 ± 46	1.70 ± 0.19 [a,b,c]	908 ± 7 [a,b,c]
Distal femoral epiphysis					
Base	5.75 ± 0.85	195 ± 23	291 ± 36	0.32 ± 0.10	971 ± 8
Ctrl	5.32 ± 0.41	212 ± 16	206 ± 35 [a]	0.22 ± 0.24	987 ± 10 [a]
BTX	4.62 ± 0.53 [a,b]	228 ± 21 [a,b]	305 ± 51 [b]	1.16 ± 0.14 [a,b]	925 ± 13 [a,b]
BTX+Zol	5.65 ± 0.48 [c]	199 ± 16 [c]	218 ± 22 [a,c]	0.20 ± 0.12 [c]	989 ± 10 [a,c]

16-week-old C57BL/6J female mice immobilized with botulinum toxin (BTX) and treated with zoledronic acid (Zol) compared with baseline (Base) and control (Ctrl) mice. Trabecular number (Tb.N), trabecular spacing (Tb.Sp), connectivity density (Conn.D), structure model index (SMI), tissue mineral density (TMD), and hydroxyapatite (HA). [a] denotes a significant difference (p<0.05) from Base, [b] denotes a significant difference (p<0.05) from Ctrl, and [c] denotes a significant difference (p<0.05) from BTX. Mean ± SD.

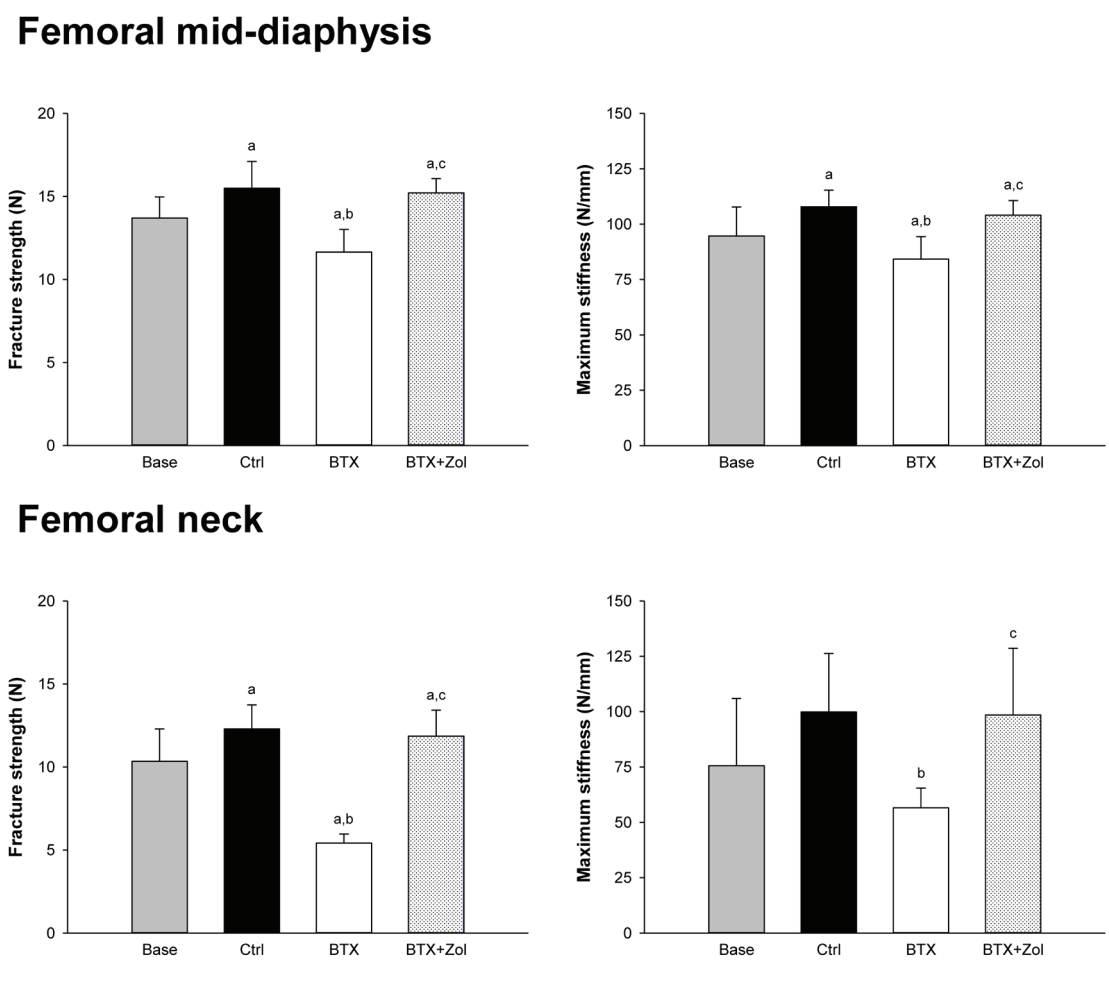

Figure 4. 16-week-old C57BL/6J female mice immobilized with botulinum toxin (BTX) and treated with zoledronic acid (Zol) compared with baseline (Base) and control (Ctrl) mice. Fracture strength and maximum stiffness acquired by mechanically testing the femoral mid-diaphysis and neck. [a] denotes a significant difference ($p<0.05$) from Base, [b] denotes a significant difference ($p<0.05$) from Ctrl, and [c] denotes a significant difference ($p<0.05$) from BTX. Mean ± SD.

Table 5. Dynamic bone histomorphometry of the distal femoral metaphysis and epiphysis.

	Day 9–13			Day 13–17		
	MS/BS (%)	MAR (µm/d)	BFR/BS (µm³/µm²/d)	MS/BS (%)	MAR (µm/d)	BFR/BS (µm³/µm²/d)
Distal femoral metaphysis						
Base	–	–	–	–	–	–
Ctrl	48.7 ± 9.3	1.91 ± 0.35	0.92 ± 0.17	54.9 ± 8.1	2.07 ± 0.29	1.13 ± 0.20
BTX	33.3 ± 4.8 [b]	2.17 ± 0.26	0.72 ± 0.15 [b]	47.3 ± 3.6 [b]	2.33 ± 0.27 [b]	1.10 ± 0.14
BTX+Zol	32.3 ± 6.6 [b]	1.09 ± 0.19 [b,c]	0.35 ± 0.10 [b,c]	29.7 ± 8.0 [b,c]	1.40 ± 0.18 [b,c]	0.42 ± 0.13 [b,c]
Distal femoral epiphysis						
Base	–	–	–	–	–	–
Ctrl	63.3 ± 11.6	1.17 ± 0.15	0.74 ± 0.15	57.6 ± 11.9	1.18 ± 0.17	0.67 ± 0.13
BTX	49.1 ± 7.5 [b]	1.49 ± 0.16 [b]	0.73 ± 0.13	62.0 ± 6.4	1.69 ± 0.18 [b]	1.04 ± 0.14 [b]
BTX+Zol	20.1 ± 7.1 [b,c]	0.75 ± 0.23 [b,c]	0.15 ± 0.07 [b,c]	17.6 ± 3.9 [b,c]	1.20 ± 0.32 [c]	0.21 ± 0.06 [b,c]

16-week-old C57BL/6J female mice immobilized with botulinum toxin (BTX) and treated with zoledronic acid (Zol) compared with baseline (Base) and control (Ctrl) mice. Mineralizing surfaces (MS/BS), mineral apposition rate (MAR), and bone formation rate (BFR/BS). [b] denotes a significant difference ($p<0.05$) from Ctrl and [c] denotes a significant ($p<0.05$) difference from BTX. Mean ± SD.

Dynamic bone histomorphometry

At the distal femoral metaphysis, during day 9-13 of the study, the injection of BTX resulted in a lower BFR/BS due to a lower MS/BS, compared to the Ctrl group (Table 5). During day 13-17, the BFR/BS of the BTX group was similar to that of the Ctrl group. Treatment with Zol lowered bone formation compared to both the BTX and Ctrl groups (Table 5).

At the distal femoral epiphysis, during day 9-13 of the study, BFR/BS was not influenced by BTX, as the MS/BS was lower and MAR higher, compared to the Ctrl group (Table 5). During day 13-17, BFR/BS in the BTX group was higher than in the Ctrl group, which was propelled by a higher MAR. Similar to the distal femoral metaphysis, Zol strongly suppressed bone formation compared to both the BTX and Ctrl groups at the femoral epiphysis (Table 5).

Reverse transcription real-time quantitative polymerase chain reaction (RT-qPCR)

At the distal part of the tibia at the time of euthanasia, *Bglap* was higher expressed in the BTX group than in the Base and Ctrl groups (Figure 5). Notably, and in agreement with dynamic bone histomorphometry, treatment with Zol suppressed the expression of *Bglap* compared to the Base, Ctrl, and BTX groups. Both the BTX and BTX+Zol groups had a higher *Rankl/Opg* ratio compared to the Base and Ctrl groups. Interestingly, *Ctsk, Nfatc1,* and *Dcstamp* was all higher expressed in the BTX+Zol group than in the Base, Ctrl, and BTX groups (Figure 5), even though Zol treatment effectively prevented BTX-induced bone resorption.

Discussion

A single injection of Zol effectively prevented BTX-induced disuse osteopenia. Furthermore, gene expression markers of osteoclastic differentiation and activity were increased in the Zol treated group, indicating that, *in vivo*, Zol only affect mature bone resorbing osteoclasts.

Zoledronic acid effectively prevents disuse osteopenia

The present study agrees with previous pre-clinical studies, were Zol consistently has been shown to either inhibit or prevent bone loss in different conditions, e.g. ovariectomy-induced osteopenia, immobilization, inflammation, and lactation[20-23]. We found that Zol prevented the BTX-induced loss of cortical and trabecular bone. Interestingly, at the distal femoral metaphysis, Zol increased BV/TV and resulted in a more plate-like trabecular network. We have previously shown that the age-related bone loss is much more evident at the distal femoral metaphysis than at the distal femoral epiphysis in C57BL/6 mice, which indicates that bone turnover is much higher at the distal femoral metaphysis[24]. Therefore, a possible explanation for the increase in BV/TV at the distal femoral metaphysis is that it contains a larger remodeling space, which is refilled after the injection of Zol due to coupling between osteoclasts and osteoblasts[25].

It has been speculated that Zol increases differentiation and activity of osteoblasts, but the findings are conflicting[26-28]. We found no indications that Zol increases osteoblastic activity using either dynamic bone histomorphometry or gene expression. However, our analyses were primarily performed on bone in which bone formation is remodeling-based. Remodeling is initiated by bone resorption followed by bone formation, and as bone resorption is inhibited by Zol, remodeling-based bone formation is therefore inhibited too. Consequently, the hypothesized Zol-induced increase in bone formation might be evident at periosteal surfaces where modeling-based bone formation takes place, which is uncoupled from bone resorption. In the present study, we

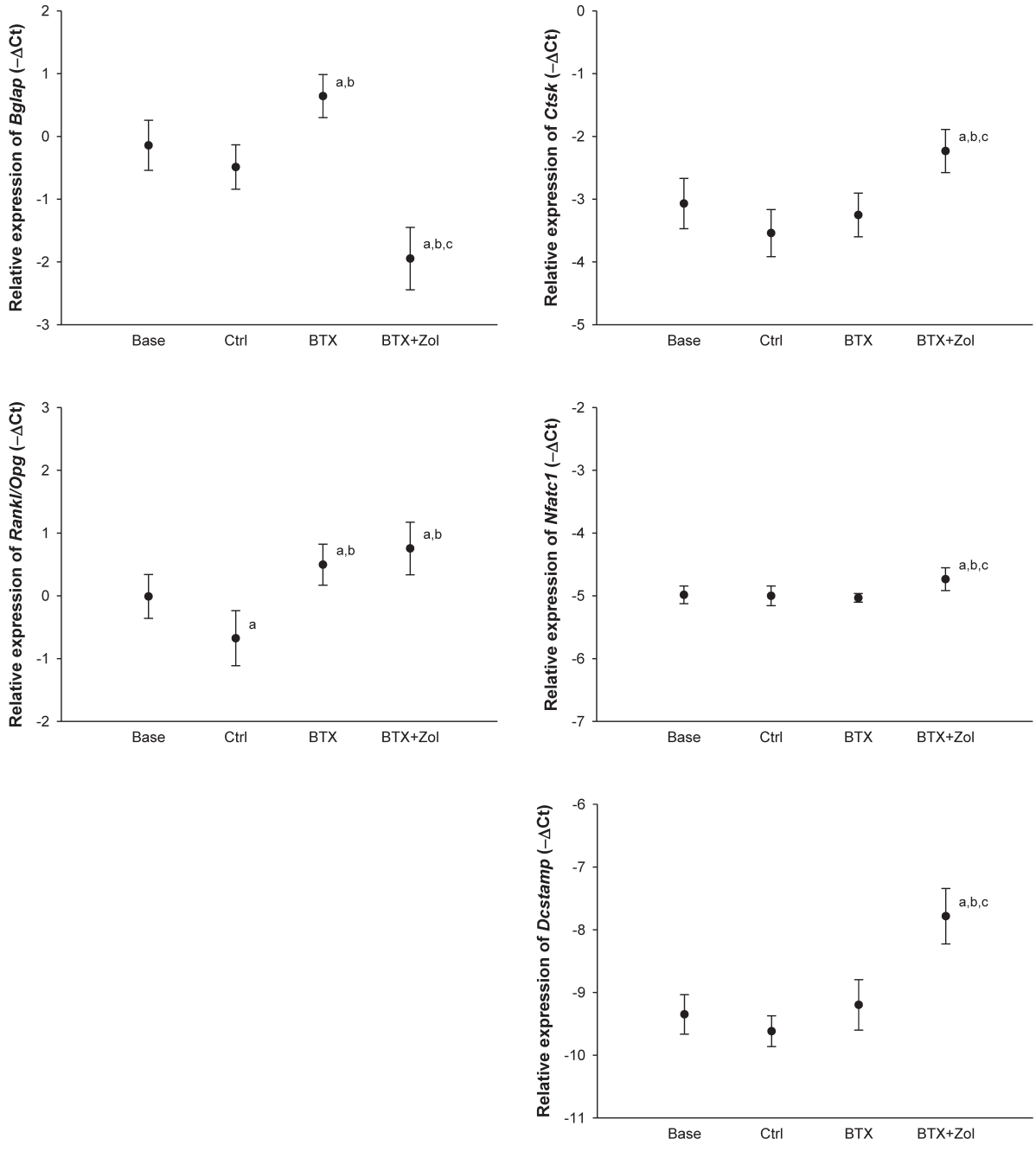

Figure 5. 16-week-old C57BL/6J female mice immobilized with botulinum toxin (BTX) and treated with zoledronic acid (Zol) compared with baseline (Base) and control (Ctrl) mice. Relative gene expression of *Bglap* (osteocalcin), *Ctsk* (cathepsin K), *Rankl/Opg-ratio* (Receptor activator of nuclear factor κ-β ligand/Osteoprotegerin-ratio), *Nfatc1* (Nuclear factor of activated T-cells, cytoplasmic 1), and *Dcstamp* (Dendrocyte expressed seven transmembrane protein) obtained from the distal part of the tibia. Mean ± SD. [a] denotes a significant difference ($p<0.05$) from Base, [b] denotes a significant difference ($p<0.05$) from Ctrl, and [c] denotes a significant difference ($p<0.05$) from BTX. Mean ± SD.

observed a trend towards decreased Tt.Ar at the femoral mid-diaphysis in the BTX-injected mice, which Zol treatment did not influence. Moreover, we have previously shown that Zol does not influence a BTX-induced lower periosteal BFR/BS in growing rats[21]. Taken together, Zol does not seem to directly influence osteoblastic activity and bone formation during disuse. However, disuse is associated with an increased secretion of sclerostin from osteocytes thereby inhibiting osteoblastic activity[29]. Therefore, an alternative or a partly explanation for the Zol-induced lower bone formation might

be that while disuse-induced bone resorption is inhibited by ZoI, the osteocytic sclerostin production is continuously increased and accounts for the reduction in bone formation. Accordingly, sclerostin has been shown to be elevated in anti-RANKL antibody treated OPG$^{-/-}$ mice and in ZoI treated post-menopausal osteoporosis[30,31]. We have previously found that it is difficult to detect disuse-induced differences in *Sost* (sclerostin) gene expression with the method at hand, and we have therefore refrained from investigating Sost expression in the present study[10].

Paretic stroke patients are at increased risk of developing osteoporosis and are as a consequence experiencing fragility fractures[32,33]. It has been shown that a single infusion of ZoI prevents the stroke-associated bone loss in both pre-clinical and clinical studies[34,35]. However, the indication for BP treatment of children with cerebral palsy and disabling neuromuscular diseases is less clear, although these patients are also at increased risk of sustaining fragility fractures[36]. This is especially due to unknown long-term effects and safety of BP treatment[37]. Currently, clinical studies are performed to validate ZoI efficacy and safety in children[38]. The present study showed that ZoI is effective in preventing disuse-induced bone loss in growing mice and, therefore, supports future clinical studies in children with disabling diseases.

Zoledronic acid does not affect osteoclastogenesis during disuse

BPs have been suggested to directly influence osteoclastogenesis, but these suggestions are based on *in vitro* studies[15-17]. Therefore, we decided to investigate how osteoclastogenesis is affected by ZoI during disuse in mice. We hypothesized that gene expression of markers of osteoclastic differentiation are augmented when disuse-induced bone resorption is inhibited by ZoI as osteoclasts are furiously produced in an attempt to resorb bone. The present study showed that the expression of *Nfatc1* and *Dcstamp*, which are markers of osteoclastic differentiation[39,40], are increased during disuse in ZoI treated mice. This suggests that osteoclastogenesis takes place in the presence of *in vivo* relevant concentrations of ZoI. Accordingly, a previous report states that ZoI increases the number of pre-mature, none bone-attached osteoclasts in intact mice[41]. Furthermore, the osteocytic network is believed to be the prime source of osteoclast-maturing factors during disuse[42-44]. Since osteoclastic differentiation takes place in ZoI treated mice, this indicates that mechanosensation of the osteocytic network is intact, and that the osteocytes desperately attempt to induce bone resorption in response to disuse.

During disuse, ZoI seems to increase the amount of mature osteoclasts based on the expression of *Ctsk*, which is an mRNA translated into the bone degrading protease cathepsin K and represents an enzyme of the bone resorbing osteoclast[45]. However, ZoI prevented BTX-induced disuse osteopenia and the higher expression of *Ctsk* might indicate that an increased number of mature osteoclasts attempts to resorb bone, but are inhibited when tasting the bone matrix. Therefore, the higher *Ctsk* expression should be viewed as a marker of the impressive and tireless mechano-adaptiveness of bone that was obstructed by ZoI in the present study. In accordance, previous studies have shown that BP treatment increases the numbers of osteoclasts attached to the bone surface during conditions that involve increased bone resorption, although bone resorption is inhibited[46,47]. However, the current findings are preliminary and calls for further studies.

Limitations and future perspective

Immunohistochemically, osteoclasts are usually identified as TRAP^{+} or CTSK^{+} multinucleated cells located in a resorption pit. Unfortunately, in the present study we were not able to produce antibody-stained histological slides of sufficient quality to reliably estimate osteoclastic morphology and numbers. The signal-to-noise ratio between osteoclasts and non-osteoclastic bone-attached cells was simply too poor. Moreover, as ZoI inhibits osteoclastic resorption it is unlikely that osteoclasts are found in a resorption pit in ZoI treated bone. Therefore, we have omitted any histological data regarding osteoclasts in the current paper.

In order to confirm our findings, it would be interesting to estimate the number of osteoclast progenitors in the bone marrow by e.g. flow cytometry. Furthermore, *in vivo* µCT would be able to ascertain whether ZoI inhibits bone resorption efficiently by estimating resorbing bone surfaces and thereby quantify osteoclastic activity.

It is not straightforward to interpret the significance of the increase in gene expression of osteoclast differentiation markers during ZoI treated disuse osteopenia. However, altered homeostasis of osteoclast differentiation and related cytokines might be a piece in the puzzle as to how BPs affect other cells in the bone marrow, e.g. adipocytes and osteoblasts as earlier suggested[48]. Specifically, it is speculated whether the hematopoietic and mesenchymal stem cell niche affect each other. This might eventually explain how manipulation of osteoclasts with BPs affect the mesenchymal stem cell linage, i.e. adipocytes and osteoblasts. However, further research is needed to establish any causal relationships.

Conclusion

BTX-induced disuse resulted in a profound bone loss that was evident at both cortical and trabecular bone sites. Treatment with ZoI prevented the disuse induced bone loss. Moreover, ZoI increased gene expression markers of osteoclastic differentiation and activity, suggesting that mechanosensation of the osteocytic network, production of pro-osteoclastic factors, and differentiation of osteoclasts are unaffected by ZoI. However, the current findings are preliminary and calls for further studies.

Acknowledgements

JBV, AB, and JST designed the study and interpreted the data; JBV acquired and analyzed the data; JBV drafted the manuscript; JBV, AB, and JST revised and approved the final version of the manuscript. All

authors are responsible for the accuracy and integrity of the work.

The authors are grateful for the hard work and excellent technical assistance of Jytte Utoft. We thank Visiopharm for the contribution to the newCAST stereology software system and the VELUX Foundation for the donation of the μCT scanner. The study was kindly supported by Helga and Peter Kornings Foundation, Lægе Søren Segel and hustru Johanne Wiibroe Segels Reseach Foundation, Inge og Per Refshalls Research Foundation, and Direktør Jacob Madsen og hustru Olga Madsens Foundation.

References

1. Rantakokko J, Uusitalo H, Jämsä T, Tuukkanen J, Aro HT, Vuorio E. Expression profiles of mRNAs for osteoblast and osteoclast proteins as indicators of bone loss in mouse immobilization osteopenia model. J Bone Miner Res 1999;14(11):1934-1942.
2. Simske SJ, Greenberg AR, Luttges MW. Effects of suspension-induced osteopenia on the mechanical behaviour of mouse long bones. J Mater Sci Mater Med 1991;2(1):43-50.
3. Sakai A, Nakamura T, Tsurukami H, Okazaki R, Nishida S, Tanaka Y, Norimura T, Suzuki K. Bone marrow capacity for bone cells and trabecular bone turnover in immobilized tibia after sciatic neurectomy in mice. Bone 1996;18(5):479-486.
4. Warner SE, Sanford DA, Becker BA, Bain SD, Srinivasan S, Gross TS. Botox induced muscle paralysis rapidly degrades bone. Bone 2006;38(2):257-264.
5. Rossetto O, Pirazzini M, Montecucco C. Botulinum neurotoxins: genetic, structural and mechanistic insights. Nat Rev Microbiol 2014;12(8):535-549.
6. Chappard D, Chennebault A, Moreau M, Legrand E, Audran M, Basle MF. Texture analysis of X-ray radiographs is a more reliable descriptor of bone loss than mineral content in a rat model of localized disuse induced by the clostridium botulinum toxin. Bone 2001; 28(1):72-79.
7. Grimston SK, Silva MJ, Civitelli R. Bone loss after temporarily induced muscle paralysis by botox is not fully recovered after 12 weeks. Ann N Y Acad Sci 2007; 1116:444-460.
8. Manske SL, Boyd SK, Zernicke RF. Muscle and bone follow similar temporal patterns of recovery from muscle-induced disuse due to botulinum toxin injection. Bone 2010;46(1):24-31.
9. Lodberg A, Vegger JB, Jensen MV, Larsen CM, Thomsen JS, Brüel A. Immobilization induced bone loss is strain specific in mice. Bone Reports 2015;2:59-67.
10. Vegger JB, Brüel A, Dahlgaard AF, Thomsen JS. Alterations in gene expression precede sarcopenia and osteopenia in botulinum toxin immobilized mice. J Musculoskelet Neuronal Interact 2016;16(4):355-368.
11. Marchand-Libouban H, Le Drévo MA, Chappard D. Disuse induced by botulinum toxin affects the bone marrow expression profile of bone genes leading to a rapid bone loss. J Musculoskelet Neuronal Interact 2013;13(1):27-36.
12. Laurent MR, Jardí F, Dubois V, Schollaert D, Khalil R, Gielen E, Carmeliet G, Claessens F, Vanderschueren D. Androgens have antiresorptive effects on trabecular disuse osteopenia independent from muscle atrophy. Bone 2016;93:33-42.
13. Camacho PM, Petak SM, Binkley N, Clarke BL, Harris ST, Hurley DL, Kleerekoper M, Lewiecki EM, Miller PD, Narula HS, Pessah-Pollack R, Tangpricha V, Wimalawansa SJ, Watts NB. American association of clinical endocrinologists and american college of endocrinology clinical practice guidelines for the diagnosis and treatment of postmenopausal osteoporosis - 2016. Endocr Pract 2016;(9)22:1111-1118.
14. Rogers MJ, Crockett JC, Coxon FP, Mönkkönen J. Biochemical and molecular mechanisms of action of bisphosphonates. Bone 2011;49(1):34-41.
15. Sudhoff H, Jung JY, Ebmeyer J, Faddis BT, Hildmann H, Chole RA. Zoledronic acid inhibits osteoclastogenesis *in vitro* and in a mouse model of inflammatory osteolysis. Ann Otol Rhinol Laryngol 2003;112(9 Pt 1):780-786.
16. Kwak HB, Kim JY, Kim KJ, Choi MK, Kim JJ, Kim KM, Shin YI, Lee MS, Kim HS, Kim JW, Chun CH, Cho HJ, Hong GY, Juhng SK, Yoon KH, Park BH, Bae JM, Han JK, Oh J. Risedronate directly inhibits osteoclast differentiation and inflammatory bone loss. Biol Pharm Bull 2009;32(7):1193-1198.
17. Kimachi K, Kajiya H, Nakayama S, Ikebe T, Okabe K. Zoledronic acid inhibits RANK expression and migration of osteoclast precursors during osteoclastogenesis. Naunyn Schmiedebergs Arch Pharmacol 2011; 383(3):297-308.
18. Bouxsein ML, Boyd SK, Christiansen BA, Guldberg RE, Jepsen KJ, Müller R. Guidelines for assessment of bone microstructure in rodents using micro-computed tomography. J Bone Miner Res 2010;25(7):1468-1486.
19. Mosekilde L, Thomsen JS, Orhii PB, McCarter RJ, Mejia W, Kalu DN. Additive effect of voluntary exercise and growth hormone treatment on bone strength assessed at four different skeletal sites in an aged rat model. Bone 1999;24(2):71-80.
20. Glatt M, Pataki A, Evans GP, Hornby SB, Green JR. Loss of vertebral bone and mechanical strength in estrogen-deficient rats is prevented by long-term administration of zoledronic acid. Osteoporos Int 2004;15(9):707-715.
21. Vegger JB, Nielsen ES, Brüel A, Thomsen JS. Additive effect of PTH (1-34) and zoledronate in the prevention of disuse osteopenia in rats. Bone 2014;66:287-295.
22. Keller KK, Thomsen JS, Stengaard-Pedersen K, Hauge EM. Systemic but no local effects of combined zoledronate and parathyroid hormone treatment in experimental autoimmune arthritis. PLoS One 2014;9(3):e92359.
23. Wendelboe MH, Thomsen JS, Henriksen K, Vegger JB, Brüel A. Zoledronate prevents lactation induced bone loss and results in additional post-lactation bone mass in mice. Bone 2016;87:27-36.
24. Vegger JB, Brüel A, Brent MB, Thomsen JS. Disuse osteopenia induced by botulinum toxin is similar in

skeletally mature young and aged female C57BL/6J mice. J Bone Miner Metab 2017; [Epub ahead of print].
25. Pataki A, Müller K, Green JR, Ma YF, Li QN, Jee WS. Effects of short-term treatment with the bisphosphonates zoledronate and pamidronate on rat bone: A comparative histomorphometric study on the cancellous bone formed before, during, and after treatment. Anat Rec 1997;249(4):458-468.
26. Corrado A, Neve A, Maruotti N, Gaudio A, Marucci A, Cantatore FP. Dose-dependent metabolic effect of zoledronate on primary human osteoblastic cell cultures. Clin Exp Rheumatol 2011;28(6):873-879.
27. Basso FG, Silveira Turrioni AP, Hebling J, de Souza Costa CA. Zoledronic acid inhibits human osteoblast activities. Gerontology 2013;59(6):534-541.
28. Heino TJ, Alm JJ, Halkosaari HJ, Välimäki VV. Zoledronic acid *in vivo* increases *in vitro* proliferation of rat mesenchymal stromal cells. Acta Orthop 2016; 87(4):412-417.
29. Galea GL, Lanyon LE, Price JS. Sclerostin's role in bone's adaptive response to mechanical loading. Bone 2017;96:38-44.
30. Catalano A, Morabito N, Basile G, Brancatelli S, Cucinotta D, Lasco A. Zoledronic acid acutely increases sclerostin serum levels in women with postmenopausal osteoporosis. J Clin Endocrinol Metab 2013;98(5):1911-1915.
31. Koide M, Kobayashi Y, Yamashita T, Uehara S, Nakamura M, Hiraoka BY, Ozaki Y, Iimura T, Yasuda H, Takahashi N, Udagawa N. Bone formation is coupled to resorption via suppression of sclerostin expression by osteoclasts. J Bone Miner Res 2017; [Epub ahead of print].
32. Ramnemark A, Nyberg L, Lorentzon R, Englund U, Gustafson Y. Progressive hemiosteoporosis on the paretic side and increased bone mineral density in the nonparetic arm the first year after severe stroke. Osteoporos Int 1999;9(3):269-275.
33. Kapral MK, Fang J, Alibhai SM, Cram P, Cheung AM, Casaubon LK, Prager M, Stamplecoski M, Rashkovan B, Austin PC. Risk of fractures after stroke: Results from the Ontario Stroke Registry. Neurology 2017;88(1):57-64.
34. Lee JI, Kim HW, Rhee WI, Park JH, Lim SH, Im S, Ko YJ. The beneficial effect of intravenous zoledronic acid therapy following an acute stroke in rats. Bone 2006; 39(2):377-382.
35. Poole KE, Loveridge N, Rose CM, Warburton EA, Reeve J. A single infusion of zoledronate prevents bone loss after stroke. Stroke 2007;38(5):1519-1525.
36. Henderson RC, Berglund LM, May R, Zemel BS, Grossberg RI, Johnson J, Plotkin H, Stevenson RD, Szalay E, Wong B, Kecskemethy HH, Harcke HT. The relationship between fractures and DXA measures of BMD in the distal femur of children and adolescents with cerebral palsy or muscular dystrophy. J Bone Miner Res 2010;25(3):520-526.
37. Boyce AM, Tosi LL, Paul SM. Bisphosphonate treatment for children with disabling conditions. PM R 2014; 6(5):427-436.
38. Bowden SA, Jessup AB, Akusoba CI, Mahan JD. Zoledronic acid in non-ambulatory children and young adults with fragility fractures and low bone mass associated with spastic quadriplegic cerebral palsy and other neuromuscular disorders. J Endocrinol Diabetes Mellit 2015;3:35-41.
39. Kim JH, Kim N. Regulation of *NFATc1* in osteoclast differentiation. J Bone Metab 2014;21(4):233-241.
40. Chiu YH, Ritchlin CT. DC-STAMP: A key regulator in osteoclast differentiation. J Cell Physiol 2016;231(11): 2402-2407.
41. Kuroshima S, Go VA, Yamashita J. Increased numbers of nonattached osteoclasts after long-term zoledronic acid therapy in mice. Endocrinology 2012;153(1):17-28.
42. Tatsumi S, Ishii K, Amizuka N, Li M, Kobayashi T, Kohno K, Ito M, Takeshita S, Ikeda K. Targeted ablation of osteocytes induces osteoporosis with defective mechanotransduction. Cell Metab 2007;5(6):464-475.
43. Xiong J, Onal M, Jilka RL, Weinstein RS, Manolagas SC, O'Brien CA. Matrix-embedded cells control osteoclast formation. Nat Med 2011;17(10):1235-1241.
44. O'Brien CA, Nakashima T, Takayanagi H. Osteocyte control of osteoclastogenesis. Bone 2013;54(2):258-263.
45. Feng X, Teitelbaum SL. Osteoclasts: New insights. Bone Res 2013;1(1):11-26.
46. Li CY, Majeska RJ, Laudier DM, Mann R, Schaffler MB. High-dose risedronate treatment partially preserves cancellous bone mass and microarchitecture during long-term disuse. Bone 2005;37(3):287-295.
47. Ralte S, Khatri K, Nagar M. Short-term effects of zoledronate on the histomorphology of osteoclast in young albino rats. Ann Anat 2011;193(6):509-515.
48. Devlin MJ, Rosen CJ. The bone-fat interface: Basic and clinical implications of marrow adiposity. Lancet Diabetes Endocrinol 2015;3(2):141-147.